Control of an *LLC* Resonant Converter Using Load Feedback Linearization

Zhijian Fang, Junhua Wang, Shanxu Duan, Kaipei Liu, and Tao Cai

***Abstract*—*LLC* resonant converter is a nonlinear system, limiting the use of typical linear control methods. This paper proposed a new nonlinear control strategy, using load feedback linearization for an *LLC* resonant converter. Compared with the conventional PI controllers, the proposed feedback linearized control strategy can achieve better performance with elimination of the nonlinear characteristics. The *LLC* resonant converter's dynamic model is built based on fundamental harmonic approximation using extended describing function. By assuming the dynamics of resonant network is much faster than the output voltage and controller, the *LLC* resonant converter's model is simplified from seven-order state equations to two-order ones. Then, the feedback linearized control strategy is presented. A double loop PI controller is designed to regulate the modulation voltage. The switching frequency can be calculated as a function of the load, input voltage, and modulation voltage. Finally, a 200 W laboratory prototype is built to verify the proposed control scheme. The settling time of the *LLC* resonant converter is reduced from 38.8 to 20.4 ms under the positive load step using the proposed controller. Experimental results prove the superiority of the proposed feedback linearized controller over the conventional PI controller.**

***Index Terms*—Extended describing functions (EDFs), feedback linearization, *LLC* resonant converter, model.**

I. Introduction

DC/DC converters have been widely used in a variety of applications for many years, such as telecommunications equipment [1], power supply of computer [2], adapter of laptop [3], [4], and DC motor drivers [5]. Nowadays, dc/dc converters are being employed for renewable energy applications like Photovoltaics (PV) [6], [7], dc microgrid [8], and HVdc systems [9]. In all these applications, high efficiency and high power density are the main objectives for a dc/dc converter. Pulse width modulation (PWM) and resonant modulation are two main types of the dc/dc converters. Due to the capability of achieving zero voltage switching (ZVS) or zero current switching (ZCS) [10], the resonant converters can work at a very high switching frequency, reducing the transformer and filter's dimensions and weights and achieve a high efficiency. Therefore, resonant converters are receiving more and more attentions.

Current papers report several popular types of resonant converters. Series resonant converters (SRC), consisting of series inductor and capacitor, can regulate the output voltage by controlling the switching frequency. High efficiency can be obtained due to achieving ZVS. However, the SRCs have poor characteristics under no-load and short-circuit conditions. They are usually used for the high voltage and low current applications. Parallel resonant converters (PRC) can solve these problems using the parallel capacitor. But the appearance of large circulating resonant currents will result in large power losses even under no-load condition. They are usually used for narrow voltage range applications. In order to overcome the drawbacks of the SRC and PRC, series–parallel resonant converters are proposed, which add a parallel capacitor. They can operate in a wide voltage range with a high efficiency. But the circulating resonant current is still large especially when the converter works away from the resonant point. The *LLC* resonant converters are multiple resonant converters containing series resonant inductor, capacitor, and parallel magnetic inductor. ZVS at the primary side and ZCS at the secondary side are realized. High efficiency and power density are achieved. Moreover, *LLC* resonant converter can work in a wide voltage range with a comparatively small switching frequency's variation. These are very advantageous especially when dealing with renewable energy and battery charging applications. Hence, the *LLC* resonant converters are becoming quite popular in industrial electronics and front-end applications.

However, the *LLC* resonant converter is a nonlinear system. Controlling an *LLC* converter is more difficult than a PWM converter due to the complex nonlinear model. The state space averaging method is widely used to model the PWM converters [11]. But the modulation signals' frequency should be much smaller than switching frequency in these methods, which are not satisfied in the *LLC* resonant converter. Fundamental harmonic approximation (FHA) and steady-state models can provide good insights into the converter behavior and overall the steady-state gain. But they cannot provide dynamic characteristics to guide the controller design [12]–[15]. Some researches use the simulation results to build the converter model [16], [17]. However, they cannot provide enough model information for designing the controller of *LLC* converter. Small signal

Manuscript received June 11, 2016; revised September 15, 2016 and December 12, 2016; accepted February 13, 2017. Date of publication February 22, 2017; date of current version October 6, 2017. This work was supported in part by the National Natural Science Foundation of China under Project 51507114, and in part by the Natural Science Foundation of Hubei Province of China under Project 2014CFB272. Recommended for publication by Associate Editor J. A. Oliver. *(Corresponding author: J. Wang.)*

Z. Fang, J. Wang, and K. Liu are with the School of Electrical Engineering, Wuhan University, Wuhan 430072, China (e-mail: fzj@whu.edu.cn; junhuawang@whu.edu.cn; kpliu@whu.edu.cn).

S. Duan and T. Cai are with the State Key Laboratory of Advanced Electromagnetic Engineering and Technology, School of Electrical and Electronic Engineering, Huazhong University of Science and Technology, Wuhan 430074, China (e-mail: duanshanxu@hust.edu.cn; caitao@hust.edu.cn).

Color versions of one or more of the figures in this paper are available online at http://ieeexplore.ieee.org.

Digital Object Identifier 10.1109/TPEL.2017.2672731

models of the *LLC* converters are built in [18] and [19], based on the extended describing function (EDF) method. In order to provide a more accuracy model, the third and fifth harmonics are considered in [20]. However, these small signal models cannot be used when the converter operation condition varies. Jinhaeng *et al.* [21], [22] build small signal models of the *LLC* converter under the worst condition to guide the controller's design. But these models limit the dynamic performance of most operation conditions. Resonant current feedback control is proposed to decrease the operation influence of the small signal model [23]. The large signal models based on EDF have been proposed for the *LLC* converter in [24]–[26]. These models provide enough dynamic information of the *LLC* converter when large signal transient disturbance occurs. But these models are still nonlinear making the control design difficult.

Linear controllers like PI and PID are applied in the *LLC* converter to achieve expected performance. Due to the limitations of small signal models, these controllers are only valid near the particular operation point. A three-pole two-zero compensation is designed in [27]–[30] to improve the dynamic characteristics in a wide input and load range. Buccella *et al.* [31] propose an observer based controller, which improves the dynamic response compared with the traditional PID controller. But these linear compensations performances are limited by the converter's nonlinearity. Some nonlinear control methods are proposed like sliding-mode control [32], bang-bang control [33], and robust control [34], [35]. They have strong robustness against parameter uncertainties and load variations. But the performance is still undesirable compared to the linear compensation. The optimal trajectory control is proposed to achieve the best dynamic performance in [36]–[39]. The variable equal load resistor values need be calculated at every instantaneous time. Meanwhile, the online computation is nonlinear and complicated. Thus, it is very difficult to implement.

In this paper, a feedback linearization controller of an *LLC* resonant converter is proposed using the load feedback strategy. A double loop controller is designed to get the modulation voltage. Then, the switching frequency is calculated as a function of the modulation voltage, input voltage, and load. The instantaneous equal load is estimated based on the output voltage and current feedback. In Section II, a nonlinear model of *LLC* resonant converter is built. Some assumptions are given in Section III and the complex *LLC* resonant converter's model is simplified from seven to two orders. In Section IV, the proposed feedback linearization control strategy is presented. Finally, the experimental results are obtained, validating the effectiveness of the proposed method.

II. Nonlinear Model of *LLC* Resonant Converter

Fig. 1 shows the circuit diagram of an *LLC* resonant converter containing three resonant components $L_{\rm r}$, $C_{\rm r}$, and $L_{\rm m}$. The power MOSFETs of the full bridge are controlled in complementary at duty 50%, ignoring the dead time and providing a square input voltage. The full-wave rectifier, together with the output capacitor, acts as a nonlinear load to provide the dc

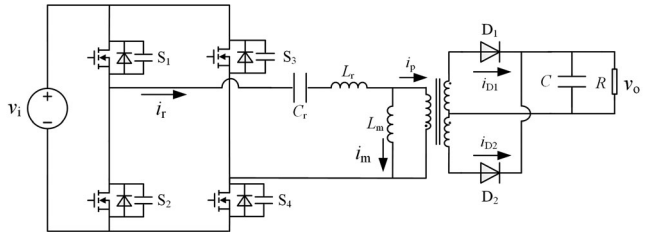

Fig. 1. Circuit diagram of an *LLC* resonant converter.

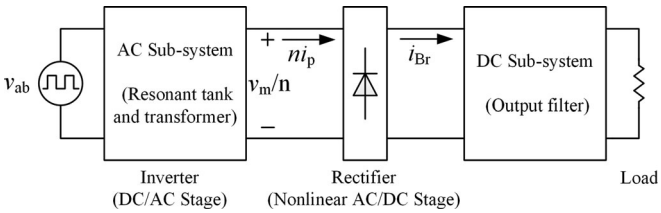

Fig. 2. Conversion stages and subsystems in an *LLC* resonant converter.

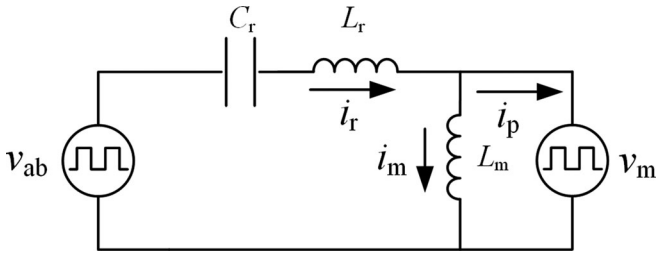

Fig. 3. Equivalent circuit diagrams of ac subsystem.

voltage. In order to analyze and design *LLC* resonant converter, the mathematical model needs to be built.

The *LLC* resonant converter can be divided into two parts: dc/ac stage and ac/dc stage, as shown in Fig. 2. The ac subsystem contains three resonant components. Using FHA, each of the three ac state variables can be decomposed into the sine and cosine components. Then, the ac subsystem is a six-order dynamic model. In the dc subsystem, the rectifier current flows through the output capacitor and load. DC subsystem is a one-order dynamic model.

A. AC Subsystem Modeling

Fig. 3 shows the equivalent circuit of the ac subsystem. The square wave voltage generated from the full bridge is applied to the resonant tank. The rectifier voltage is equal to the square wave voltage due to the large output capacitor. Based on the Kirchhoff's laws, the sate equations of *LLC* resonant converter can be obtained as follows:

$$\begin{aligned} L_r \dot{i}_r &= -v_c + v_{ab} - v_m \\ C_r \dot{v}_c &= i_r \\ L_m \dot{i}_m &= v_m \end{aligned} \tag{1}$$

where i_r, v_c, and i_m are the inductor current, capacitor voltage, and magnetic current, respectively. v_{ab} and v_m are the input and output square wave voltage.

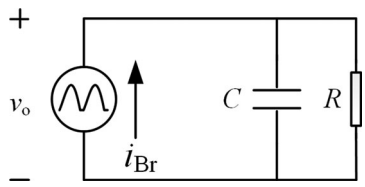

Fig. 4. Equivalent circuit diagrams of dc subsystem.

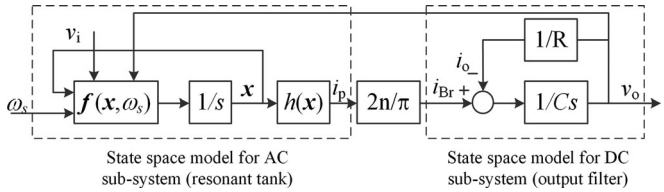

Fig. 5. Nonlinear combined system model of an *LLC* resonant converter.

Using the FHA method, the state variables, input and output voltage can be approximated as sinusoidal states with switching angle frequency ω_s, as shown in the following equation. The derived process of magnetic voltage v_m is given in the Appendix

$$\begin{aligned} i_r &= i_{rs}\sin\omega_s t + i_{rc}\cos\omega_s t \\ v_c &= v_{cs}\sin\omega_s t + v_{cc}\cos\omega_s t \\ i_m &= i_{ms}\sin\omega_s t + i_{mc}\cos\omega_s t \\ v_{ab} &= (4v_i/\pi)\sin\omega_s t \\ v_m &= [(i_{rs}-i_{ms})/i_p](4nv_o/\pi)\sin\omega_s t \\ &\quad + [(i_{rc}-i_{mc})/i_p](4nv_o/\pi)\cos\omega_s t \end{aligned} \tag{2}$$

where i_{rs}, i_{rc}, v_{cs}, v_{cc}, i_{ms}, i_{mc}, v_{ms}, v_{mc} are the sine and cosine components of the inductor current, capacitor voltage, and magnetic current and voltage. v_i and v_o are the input and output dc voltage, respectively. i_p is the primary rectifier current. n is the transformer ratio. By making use of (2) from (1), the equations of fundament components can be obtained. Since these equations are correct at every time, the coefficients of sine and cosine components must be equal, respectively. Then, the state equation of the ac subsystem can be derived

$$\begin{bmatrix} \dot{i}_{rs} \\ \dot{i}_{rc} \\ \dot{i}_{ms} \\ \dot{i}_{mc} \\ \dot{v}_{cs} \\ \dot{v}_{cc} \end{bmatrix} = \begin{bmatrix} -4(i_{rs}-i_{ms})nv_o/(\pi L_r i_p) - v_{cs}/L_r + \omega_s i_{rc} \\ +4v_i/(\pi L_r) \\ -4(i_{rc}-i_{mc})nv_o/(\pi L_r i_p) - v_{cc}/L_r - \omega_s i_{rs} \\ 4(i_{rs}-i_{ms})nv_o/(\pi L_m i_p) + \omega_s i_{mc} \\ 4(i_{rc}-i_{mc})nv_o/(\pi L_m i_p) - \omega_s i_{ms} \\ i_{rs}/C_r + \omega_s v_{cc} \\ i_{rc}/C_r - \omega_s v_{cs} \end{bmatrix}$$

$$i_p = \sqrt{(i_{rs}-i_{ms})^2 + (i_{rc}-i_{mc})^2}. \tag{3}$$

Equation (3) can be simplified as follows:

$$\begin{aligned} \dot{\mathbf{x}} &= f(\mathbf{x},\omega_s) \\ i_p &= h(\mathbf{x}) \\ \mathbf{x} &= [i_{rs}, i_{rc}, v_{cs}, v_{cc}, i_{ms}, i_{mc}]. \end{aligned} \tag{4}$$

B. DC Subsystem Modeling

Fig. 4 shows the equivalent circuit of the dc subsystem. The rectifier is equal to the current source, providing the energy for the output filter and load. i_{Br} is the average rectifier output current. Since the switching frequency is very high and the output capacitor is large, the average value is valid for modeling and analyzing the dc subsystem. The state equations of the dc subsystem are given as follows:

$$C\dot{v}_o = i_{Br} - v_o/R \tag{5}$$

where *C* is the output capacitor and *R* is the load.

C. Combined System Modeling of AC and DC

Fig. 5 shows the combined system model of the *LLC* resonant converter. The ac and dc subsystems are combined through the transform and rectifier. i_{Br} can be calculated as follows:

$$i_{Br} = 2ni_p/\pi = 2n\sqrt{(i_{rs}-i_{ms})^2 + (i_{rc}-i_{mc})^2}/\pi. \tag{6}$$

Equations (3)–(6) give the state equations of the *LLC* resonant converter.

III. Simplified Model of *LLC* Resonant Converter

In Section II, the mathematical model of an *LLC* resonant converter is built. But this model is still difficult to analyze and design the controller due to the seven-order nonlinear state equations. As shown in (3)–(6), the complexity and nonlinearity of the model are caused by the resonant network and rectifier circuit in the *LLC* resonant converter. In order to simplify the model, the influences of resonant network and rectifier must be reduced. As shown in Fig. 4, the resonant network and rectifier can be equal as a controlled current source, the controlled current i_p can be calculated as follows:

$$i_p{}^2 = (i_{rs}-i_{ms})^2 + (i_{rc}-i_{mc})^2. \tag{7}$$

The state equation of i_p can be obtained as

$$\dot{i}_p = (i_{rs}-i_{ms})(\dot{i}_{rs}-\dot{i}_{ms})/i_p + (i_{rc}-i_{mc})(\dot{i}_{rc}-\dot{i}_{mc})/i_p. \tag{8}$$

Combine (3) with (8), the state equation can be derived as follows:

$$\begin{aligned} \dot{i}_p = &-4(1/L_r + 1/L_m)nv_o/\pi \\ &+ \begin{bmatrix} 4(i_{rs}-i_{ms})v_i/\pi - \\ (i_{rs}-i_{ms})v_{cs} - (i_{rc}-i_{mc})v_{cc} \end{bmatrix} / (L_r L_p). \end{aligned} \tag{9}$$

The resonant state variables i_{rs}, i_{ms}, i_{rc}, i_{mc}, v_{cs}, and v_{cc} in the right part of (9) are decided by (3), which make the controlled current source very complex. As shown in (3), the resonant network's model has six poles and two double zeros. The dominant poles are the one beat frequency double poles. As the switching frequency moves to resonant frequency, the beat

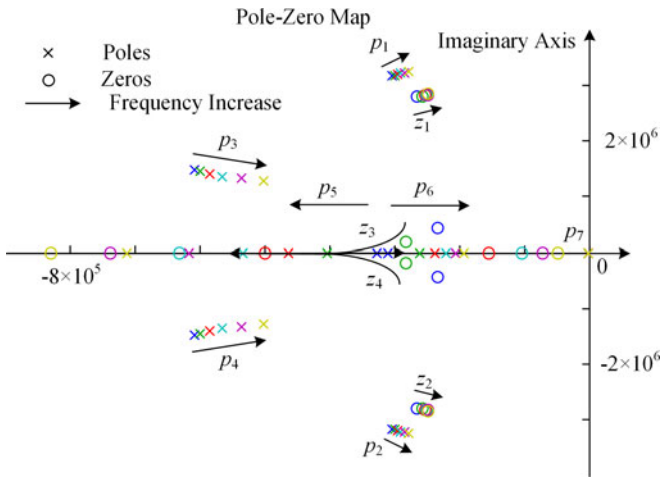

Fig. 6. Pole-zero placement of the *LLC* resonant converter small signal model.

frequency double poles will move to the lower frequency. When the switching frequency is very close to resonant frequency, the beat frequency will eventually split and becomes two real poles [40]. In the dc subsystem, there is only one pole ignoring the ESR zero, as shown in (5). In the usual *LLC* resonant converter, the resonant network's parameters are usually very small to achieve high resonant frequency. The output filter's parameters are usually very large to maintain the output voltage and current. So the dynamic of resonant network is much faster than the output voltage and controller. Therefore, the dynamics of the resonant converters can be divided into the low-frequency behavior and high-frequency behavior. The low-frequency dynamics are determined by the output capacitor, resonant impedance, and load. The high-frequency dynamic is around the beat frequency, which is the difference value between the switching frequency and the resonant frequency. The pole-zero placement of the *LLC* resonant converter of the small signal model is shown in Fig. 6. As the switching frequency increases, the six high frequency poles and four zeros move to the imaginary axis. As shown in the figure, the high frequency poles and four zeros caused by the resonant network are far away from the imaginary axis. Therefore, these high frequency poles and zeros can be ignored and the *LLC* resonant converter's model can be simplified into a two-order model.

Assume the dynamic of resonant network is much faster than the output voltage and controller. The resonant state variables can reach the steady state at the ending time of each control period. The resonant state variables, such as i_{rc}, i_{rs}, i_{mc}, i_{ms}, v_{cc}, v_{cs}, in (9) are constant values during the control period. Therefore, the last part of (9) can be equal to a voltage source

$$\dot{i}_p = 4\left(1/L_r + 1/L_m\right) n\left(v_n - v_o\right)/\pi \tag{10}$$

where v_n is the equal secondary side rectifier voltage. The ac subsystem can be equal to an ideal controllable voltage source and an inductor. The simplified equivalent circuit of *LLC* resonant converter is shown in Fig. 7. Combining (6) and (10), the

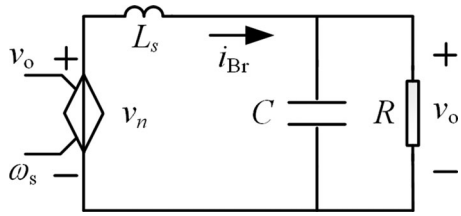

Fig. 7. Simplified equivalent circuit diagrams of an *LLC* resonant.

output equal inductor L_s can be derived as follows:

$$L_s = \pi^2/8n^2\left(1/L_r + 1/L_m\right). \tag{11}$$

The equal rectifier voltage v_n is controllable and decided by the switching frequency, resonant network, and output voltage. Since the dynamic of resonant network is much faster than the output voltage and controller, the controllable rectifier voltage v_n can reached at the steady state during every control period.

Since the switching frequency of *LLC* resonant converter is near the resonant frequency, the resonant state variables can be assumed as sinusoidal signals. The dc subsystem's load can be equal to the resister $R_{\rm eq}$. Based on FHA method, the equivalent resister is

$$R_{\rm eq} = 8n^2R/\pi^2. \tag{12}$$

Then, the expressions for the steady-state secondary rectifier voltage v_n can be achieved based on FHA analysis

$$v_n = v_i/\left(n\sqrt{(1+h-h/f^2)^2 + Q^2(f-1/f)^2}\right). \tag{13}$$

where $h = L_r/L_m$, $f = \omega_s/\omega_r$, $\omega_r = 1/\sqrt{L_rC_r}$, $Q = \sqrt{L_r/C_r}/R_{\rm eq}$.

Therefore, the steady-state value for the dc subsystem input v_n is calculated as the function of the input voltage v_i, output load *R*, and switching frequency f_s. Then, the simplified model of an *LLC* resonant converter can be achieved based on the equal circuit in Fig. 7

$$\begin{aligned} L_s\dot{i}_{Br} &= -v_o + v_n \\ C\dot{v}_o &= i_{Br} - \frac{v_o}{R}. \end{aligned} \tag{14}$$

IV. Feedback Linearization Control of an *LLC* Resonant Converter

In Section III, the simplified model of an *LLC* resonant converter is built. It is a simple two-order model. But it is still a nonlinear system due to the nonlinear function between the switching frequency and the rectifier voltage. Conventional linear control methods such as PI controllers are difficult to be applied. In order to eliminate the nonlinear characteristics, a linear feedback controller needs to be developed. As shown in (13), the rectifier voltage $v_{\rm n}$ is a nonlinear function of the switching frequency. If we can formulate an inverse function of the rectifier voltage, the nonlinear factors can be eliminated. Then, the reconstructed system can be a linear system. The conventional PI controller can be used to achieve the modulation

voltage. This paper proposes a nonlinear control strategy using the load feedback linearization to achieve a great performance of the *LLC* resonant converter.

First, we should formulate an inverse function of rectifier voltage. Define the input variable of the inverse function is the modulation voltage v_{rn}. The output variable is the switching frequency. The formulated function should be the inverse function of the rectifier voltage to make the rectifier voltage $v_{\rm n}$ linearly varying with the modulation voltage v_{rn}.

Since the input voltage and output load can be measured, (13) can be expressed as

$$v_n = M(\omega_s). \tag{15}$$

The switching frequency is calculated from the modulation voltage. Then, define the transfer function between the switching frequency and the modulation voltage as follows:

$$\omega_s = g(v_{rn}). \tag{16}$$

In order to eliminate the nonlinearity, the functions need meet the requirement of the following equation:

$$v_n = M(\omega_s) = M(g(v_{rn})) = kv_{rn} \tag{17}$$

where $g(v_{rn})$ is the inverse function of $M(\omega_s)$, and k is the proportion coefficient. The value of k does not affect the linearization process. In this paper, we assume $k = 1$. Then, the modulation voltage v_{rn} needs to meet the equation as follows:

$$v_{rn} = v_i / \left(n\sqrt{(1+h-h/f^2)^2 + Q^2(f-1/f)^2} \right). \tag{18}$$

The equation can be extended as follows:

$$f^6Q^2 + f^4\left[(1+h)^2 - 2Q^2 - (v_i/nv_{rn})^2\right] + f^2\left[Q^2 - 2h(1+h)\right] + h^2 = 0. \tag{19}$$

Define

$$\begin{aligned} x &= f^2 \\ a &= Q^2 \\ b &= (1+h)^2 - 2Q^2 - (v_i/nv_{rn})^2 \\ c &= Q^2 - 2h(1+h) \\ d &= h^2. \end{aligned} \tag{20}$$

Equation (19) can be simplified as follows:

$$ax^3 + bx^2 + cx + d = 0. \tag{21}$$

By using the Cardano formula, the equation can be solved. First, calculate sign of the discriminants of the equation

$$\begin{aligned} \Delta &= q^2/4 + p^3/27 \\ p &= \frac{3ac - b^2}{3a^2} \\ q &= \frac{2b^3 - 9abc + 27a^2d}{27a^3}. \end{aligned} \tag{22}$$

Then, the solutions of the equation can be obtained.

1) If $\Delta > 0$, one root is real and two are complex conjugates

$$\begin{aligned} x_1 &= \sqrt[3]{-\frac{q}{2} + \sqrt{\frac{q^2}{4} + \frac{p^3}{27}}} + \sqrt[3]{-\frac{q}{2} - \sqrt{\frac{q^2}{4} + \frac{p^3}{27}}} - \frac{b}{3a} \\ x_2 &= \sqrt[3]{-\frac{q}{2} + \sqrt{\frac{q^2}{4} + \frac{p^3}{27}}}\omega + \sqrt[3]{-\frac{q}{2} - \sqrt{\frac{q^2}{4} + \frac{p^3}{27}}}\omega^2 - \frac{b}{3a} \\ x_3 &= \sqrt[3]{-\frac{q}{2} + \sqrt{\frac{q^2}{4} + \frac{p^3}{27}}}\omega^2 + \sqrt[3]{-\frac{q}{2} - \sqrt{\frac{q^2}{4} + \frac{p^3}{27}}}\omega - \frac{b}{3a} \\ \omega &= \frac{-1+\sqrt{3}i}{2}. \end{aligned} \tag{23}$$

2) If $\Delta = 0$, all roots are real, and at least two are equal

$$\begin{aligned} x_1 &= \sqrt[3]{-\frac{q}{2}} + \sqrt[3]{-\frac{q}{2}} - \frac{b}{3a} \\ x_2 = x_3 &= \sqrt[3]{-\frac{q}{2}}\omega + \sqrt[3]{-\frac{q}{2}}\omega^2 - \frac{b}{3a}. \end{aligned} \tag{24}$$

3) If $\Delta < 0$, all roots are real and unequal

$$\begin{aligned} x_1 &= 2\sqrt{-\frac{p}{3}}\cos\frac{\theta}{3} - \frac{b}{3a} \\ x_2 &= 2\sqrt{-\frac{p}{3}}\cos(\frac{\theta}{3} + 120^\circ) - \frac{b}{3a} \\ x_3 &= 2\sqrt{-\frac{p}{3}}\cos(\frac{\theta}{3} - 120^\circ) - \frac{b}{3a} \\ \theta &= \arccos\frac{-q\sqrt{-27p}}{2p^2}. \end{aligned} \tag{25}$$

Finally, the switching frequency can be derived. Since the solution is the square value of the switching frequency, all the roots need to be positive. If the roots are negative or complex, no solution is existed to achieve the modulation voltage. Then, the switching frequency is forced to be resonant frequency to achieve the maximum output voltage. When the equation has solution, they may be two or one positive real roots. Generally, the maximum positive real roots are chosen to ensure that the ZVS can be achieved. Then, the switching frequency can be obtained

$$\omega_s = g(R, v_{rn}) = \begin{cases} \omega_r & \Delta > 0 \\ \omega_r\sqrt{\max(x_1, x_2, x_3)} & \Delta \le 0 \end{cases}. \tag{26}$$

The ac subsystem is fed with the switching frequency. This scheme uses the function of the output feedback to linearize the resonant converter model. The function can be implemented using the output voltage and current, as shown in Fig. 8.

By combining the nonlinear ac subsystem model, the linear dc subsystem model, and the nonlinear function, as shown in Fig. 8, the transfer function of the modulation voltage v_{rn} and

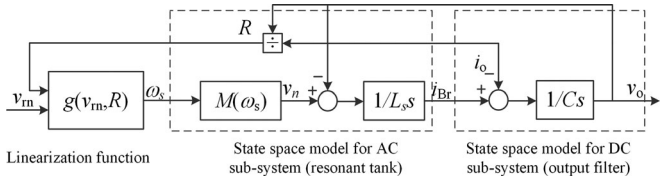

Fig. 8. Output feedback linearization control of an *LLC* resonant converter.

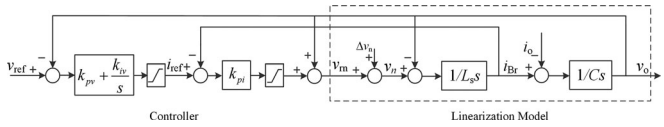

Fig. 9. Closed-loop control structure of an *LLC* resonant converter.

TABLE I
PARAMETERS OF THE *LLC* RESONANT CONVERTER

Parameter	Symbol	Value
Input voltage (V)	v_i	240
Output voltage (V)	v_o	24
Maximum output current (A)	i_o	8
Resonant capacitor (nF)	C_r	23.5 nF
Resonant inductor (μH)	L_r	86 μH
Magnetic inductor (μH)	L_m	266.5 μH
Transformer ratio	n	10:1:1
Output capacitor (μF)	C	3960
Switching frequency (kHz)	f	0–300

output voltage v_o is linear. The switching frequency ω_s satisfies (18). In order to build the transfer function from the modulation voltage to the rectifier voltage, some changes of the equations are expressed. Define $\hat{\mathbf{x}}$ is the virtual state variables, which is $[\hat{i}_{rs}, \hat{i}_{rc}, \hat{i}_{ms}, \hat{i}_{mc}, \hat{v}_{cs}, \hat{v}_{cc}]$. The virtual state variables are the variables of the inverse function $\omega_s = g(v_{rn}, R)$. They can satisfy (18). Then, the inverse function can be expressed as follows. Since the state variables are in a steady state, the gradients of these variables are zero

$$0 = f(\hat{\mathbf{x}}, \omega_s)$$

$$v_{rn} = 2nR\sqrt{\left(\hat{i}_{rs} - \hat{i}_{ms}\right)^2 + \left(\hat{i}_{rc} - \hat{i}_{mc}\right)^2}/\pi. \tag{27}$$

Define the state error between the virtual and real variables as follows:

$$\Delta\mathbf{x} = \mathbf{x} - \hat{\mathbf{x}}. \tag{28}$$

The state equation of error can be achieved from (4) and (27)

$$\Delta\dot{\mathbf{x}} = f(\Delta\mathbf{x}, \omega_s). \tag{29}$$

Since the dynamic of resonant network is much faster than the output voltage and the controller, the state error reaches at steady state during every control period. The transfer function from the modulation voltage to the rectifier voltage can be achieved as follows:

$$v_n = v_{rn}. \tag{30}$$

Combining (14) with (30), the linearized model of an *LLC* resonant converter in Fig. 8 can be expressed as follows:

$$C\dot{v}_o = i_{Br} - v_o/R$$

$$L_s\dot{i}_{Br} = v_{rn} - v_{o.} \tag{31}$$

Such a simplified two-order model cannot replace the derived model, which provides detailed dynamics of an *LLC* resonant converter. But it is useful for simplifying the controller design.

The *LLC* resonant converter has been linearized using the load feedback linearization. Then, we can design a conventional PI controller to achieve the modulation voltage. The *LLC* resonant converter is designed as a voltage source. The output voltage should be regulated. Then, the output voltage is used for the feedback in the control scheme. The control structure is shown in Fig. 9.

The rms value of resonant current is measured as the inner loop feedback. Δv_n is the disturbance between the modulation voltage and the rectifier voltage, which is caused by the measurement error of the resonant parameters. The proportional gain k_{pi} is designed to damp the oscillatory response and limit the maximum resonant current. The output voltage is added to the output value of the controller for better dynamic performance. Then, the inner loop transfer function can be derived

$$G_i = k_{pi}/(L_s s + k_{pi}). \tag{32}$$

A PI controller is applied in the outer loop feedback to regulate the output voltage. The closed-loop transfer function of an *LLC* resonant converter can be achieved

$$G = \frac{v_o}{v_{\text{ref}}} = \frac{G_i(k_{pv}s + k_{iv})}{Cs^2 + G_i(k_{pv}s + k_{iv})} = \frac{k_{pi}k_{pv}s + k_{pi}k_{iv}}{L_sCs^3 + k_{pi}Cs^2 + k_{pi}k_{pv}s + k_{pi}k_{iv}}. \tag{33}$$

where k_{pv} and k_{iv} are the integral and proportional gain of the out loop, respectively. Using the method of zero-poles assignment, the values of k_{pv} and k_{iv} can be achieved. Then, the fluctuation transfer function can be achieved

$$v_o = \Delta v_n s/\left(L_sCs^3 + k_{pi}Cs^2 + k_{pi}k_{pv}s + k_{pi}k_{iv}\right). \tag{34}$$

The steady value of the fluctuation transfer function is zero. Thus, the influence of parameter fluctuations can be eliminated.

V. SIMULATION AND EXPERIMENTAL RESULTS

In order to verify the effectiveness of the proposed model and control method, a simulation model of full-bridge *LLC* resonant converter has been built in MATLAB. The specifications of the parameters used for the simulation are given in Table I.

In order to verify the accuracy of the simplified model, the bode plots of the full order and reduced order models are given in Fig. 10.

In Fig. 10, the blue and red lines represent full order and simplified model, respectively. It can be seen that in low and medium frequency range, two models have similar frequency characteristics. The simplified model is accurate enough to guide the controller design. However, in the high frequency range (near the switching frequency), the simplified model shows its merits

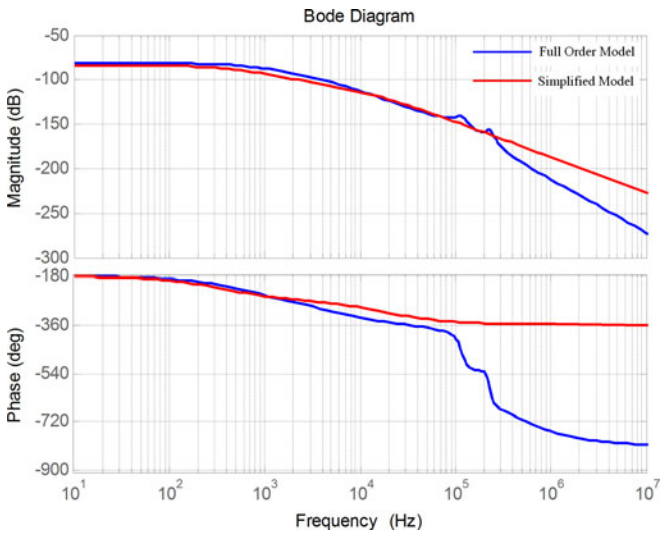

Fig. 10. Bode plots of full order and reduced simplified model.

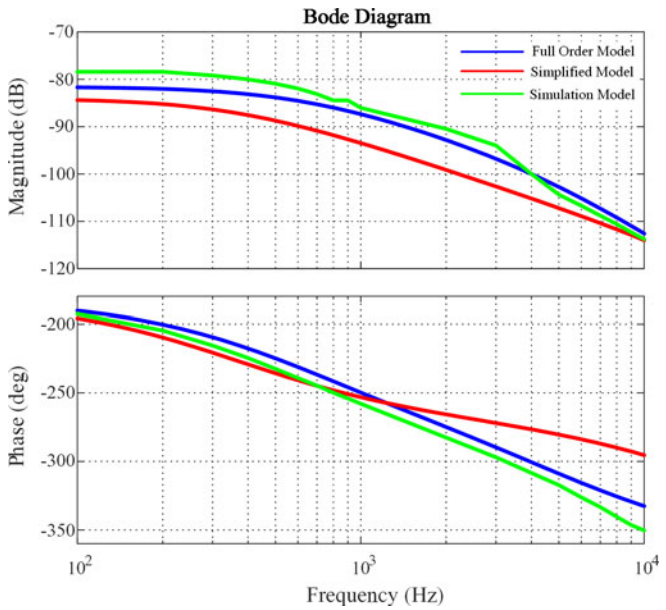

Fig. 11. Bode plots of simulation mode, full order, and simplified model.

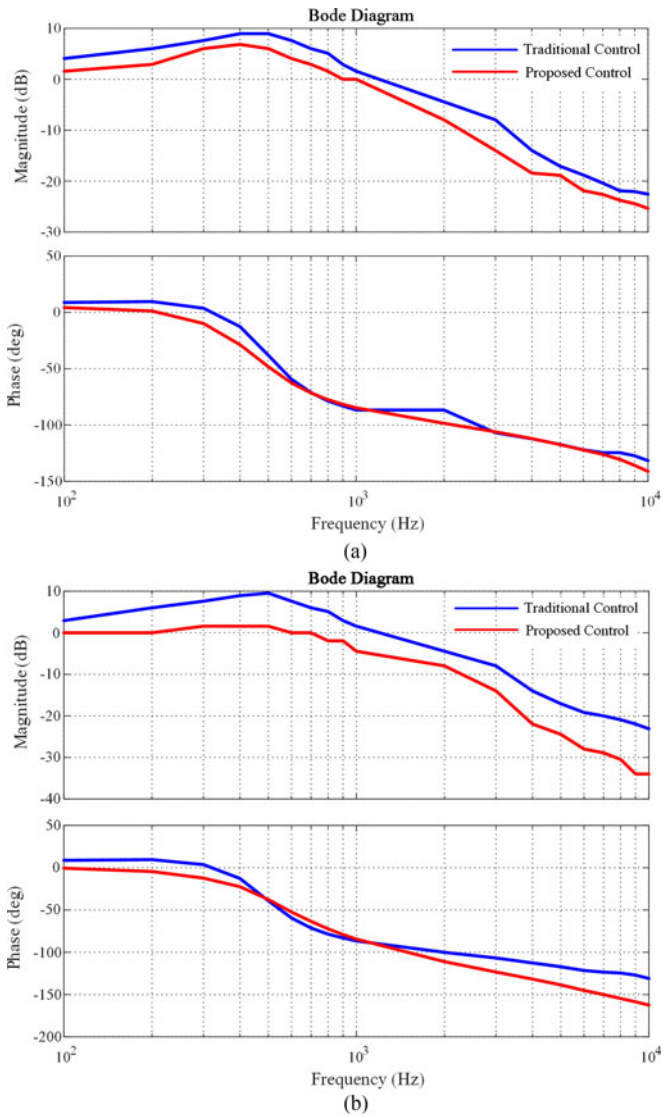

Fig. 12. Loop transfer function bode plot comparison of the traditional and proposed control scheme. (a) At full load. (b) At half load.

noticeably in which the simplified model excludes poles caused by the resonant components, which has no effects on the control performance of an *LLC* resonant converter.

Fig. 11 shows the frequency response of the simulated *LLC* resonant converter model, full-order model, and simplified model. The frequency response curves of the three models are quite similar as they obtained similar poles and zeros. Moreover, the steady-state gains of theoretical modes (full-order model and simplified model) are lower than that of simulated model due to the ignorance of harmonics. Fig. 11 proves that the simplified model can describe the frequency response of an *LLC* resonant converter efficiency.

The feedback linearization control scheme and traditional control scheme are also applied in the simulation. Fig. 12 shows the frequency response of the traditional control scheme and the proposed control scheme. In addition, comparisons between the linearized and traditional control scheme, both of which have the same PI parameters, are also implemented by simulation and Fig. 12 shows the related frequency response results.

The blue lines are the traditional control scheme and red lines are the proposed scheme. Fig. 12(a) shows the frequency response plots at full load and Fig. 12(b) shows the plots at half load. From both figures, it can be found that the proposed control scheme has lower resonant peak value and larger phase margin. The proposed control scheme can effectively improve the performance of the *LLC* resonant converter.

A 200 W laboratory prototype of a full-bridge *LLC* resonant converter has also been built. The specifications of the parameters used for the prototype are given in Table I. Fig. 13 shows the proposed control scheme of an *LLC* resonant converter. The linearization function is applied in this paper based on the typical PI controller to linearize the converter model and improve the performance.

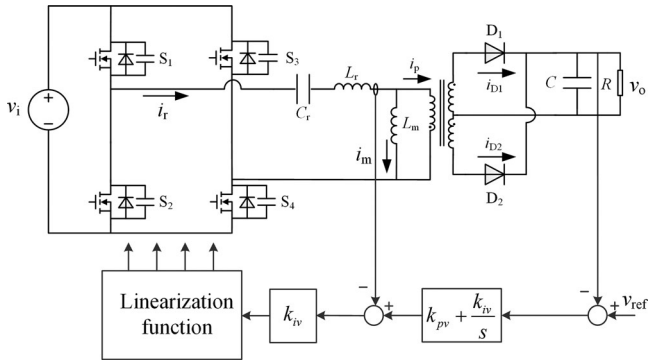

Fig. 13. Closed-loop output voltage control of an *LLC* converter using proposed linearized control.

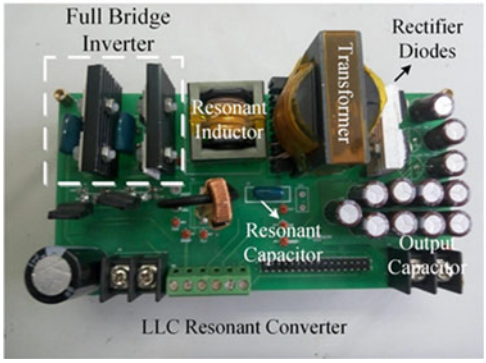

Fig. 14. Experimental setup of a 200 W *LLC* resonant converter.

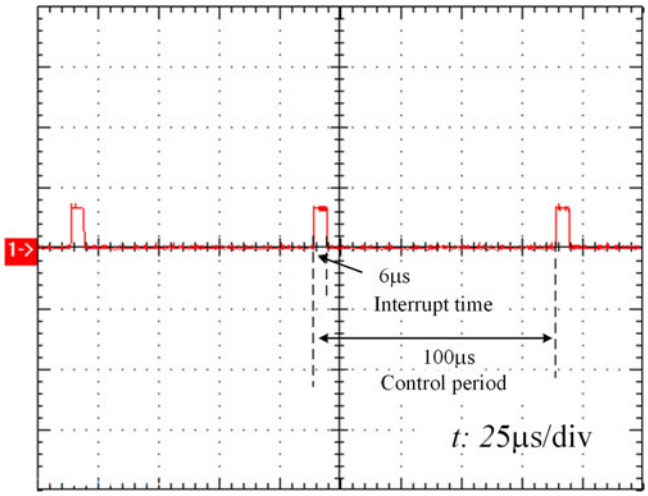

Fig. 15. Time signal waveform of interrupt function.

Texas Instruments TMS320F28335 control card, which contains a 32-b floating point DSP microcontroller, is used to implement the control scheme, produces the pulse frequency modulation for the power MOSFETs. The sample and control frequency is 10 kHz, which is lower than the switching frequency. The sample and calculation time can be ensured. Due to the influence of the interturn distributed capacitor in the transformer, the output voltage is higher than simulation results under the light load condition. Then, the burst control is applied to regulate the output voltage under no load condition. Fig. 14 shows the experimental setup of this *LLC* resonant converter.

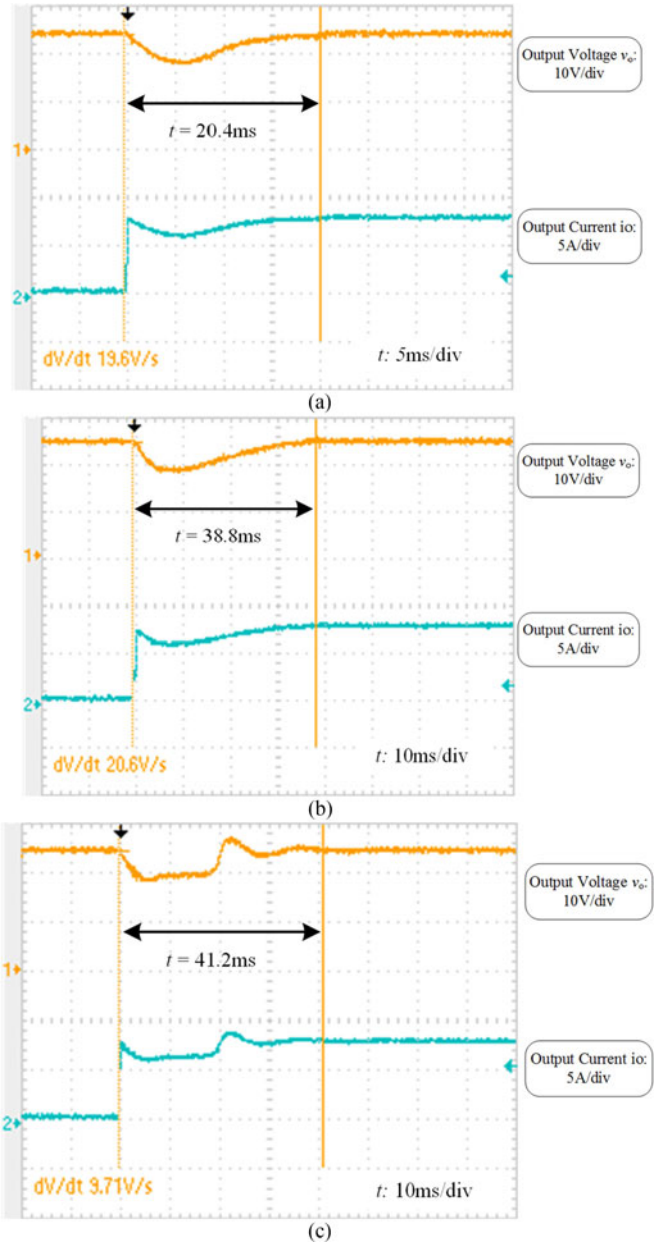

Fig. 16. Experimental results of *LLC* resonant converter against load step from no load to full load. (a) Case 1 with proposed strategy. (b) Case 2 with PI controller. (c) Case 3 with PI controller in switching frequency.

In order to accelerate the computer speed, IQ math library is used in the program code. A General-purpose input/output (GPIO) signal waveform is shown in Fig. 15 to measure the interruption time and computer time. The GPIO port is set at the beginning of interrupt function and cleared at end. The computer time of interruption function is only 6 μs. And the control period is 100 μs. The interruption percentage is only 6%. If we want to maximize the bandwidth, the interrupt percentage usually should be smaller than 60%. Then, the minimum interrupt period is 10 μs. The maximum bandwidth we can get is 100 kHz.

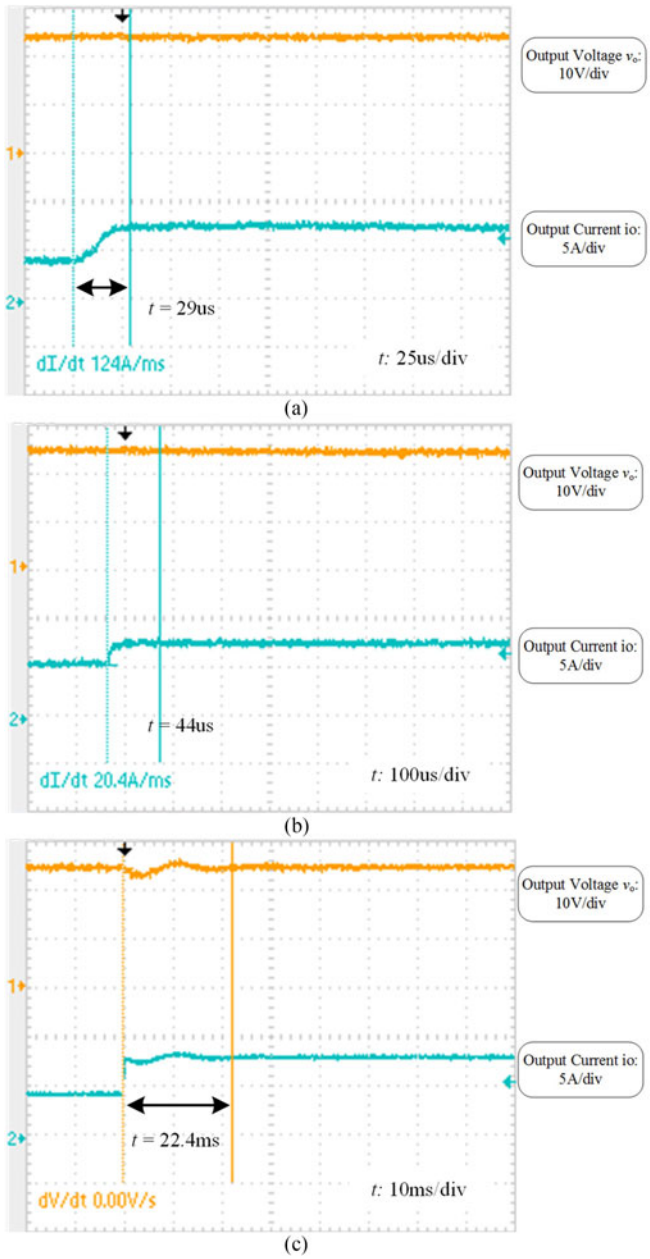

Fig. 17. Experimental results of *LLC* resonant converter against load step from half load to full load. (a) Case 1 with proposed strategy. (b) Case 2 with PI controller. (c) Case 3 with PI controller in switching frequency.

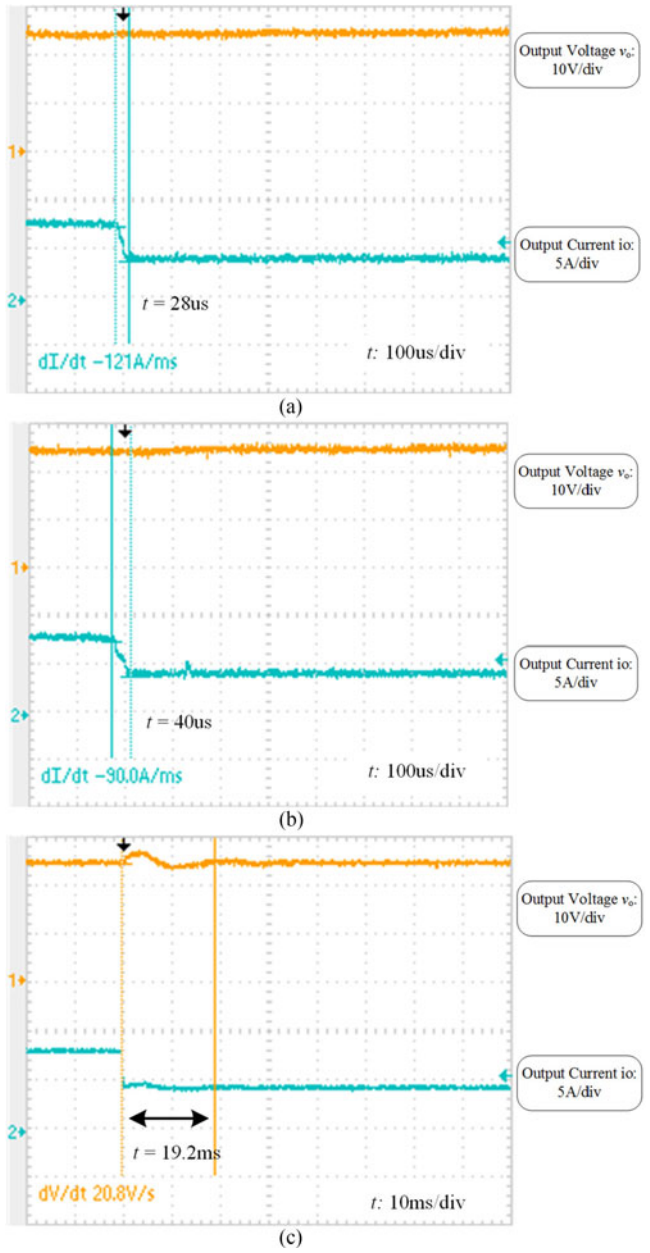

Fig. 18. Experimental results of *LLC* resonant converter against load step from full load to half load. (a) Case 1 with proposed strategy. (b) Case 2 with PI controller. (c) Case 3 with PI controller in switching frequency.

In order to verify the effectiveness of the proposed feedback linearized control strategy, the experiments of the proposed strategy with control frequency of 10 kHz (Case 1), the conventional PI controller with control frequency of 10 kHz (Case 2), and the PI controller sampling at every switching period (Case 3) are expressed. Fig 16 shows the experimental results against the step load from no load to full load in the three cases. Due to the influence of junction and winding capacitor, the output voltage is higher than the reference voltage even at maximum frequency. Then, the converter operates at burst mode to maintain the reference voltage under the light load condition. When the loads step up, the switching frequency is regulated from the maximum frequency to the expectable value. At case 1, the settling time is only 20.4 ms and voltage drop is 6 V, as shown in Fig. 16(a). Due to the complex computing, the control frequency in case 1 is only 10 kHz to ensure the enough computing time in every control period. At case 2, the setting time is 38.8 ms and the voltage drop is 6 V. The conventional PI controller's control frequency is still 10 kHz. Then, the output voltage can reach at steady state at the ending time of every control period. At case 3, the setting time is 41.2 ms and voltage drop is 6.4 V. At this case, the switching frequency is regulated at every switching period. Since the output voltage may not reach steady state at every switching period, some oscillations occur. The dynamic response is worse than case 2.

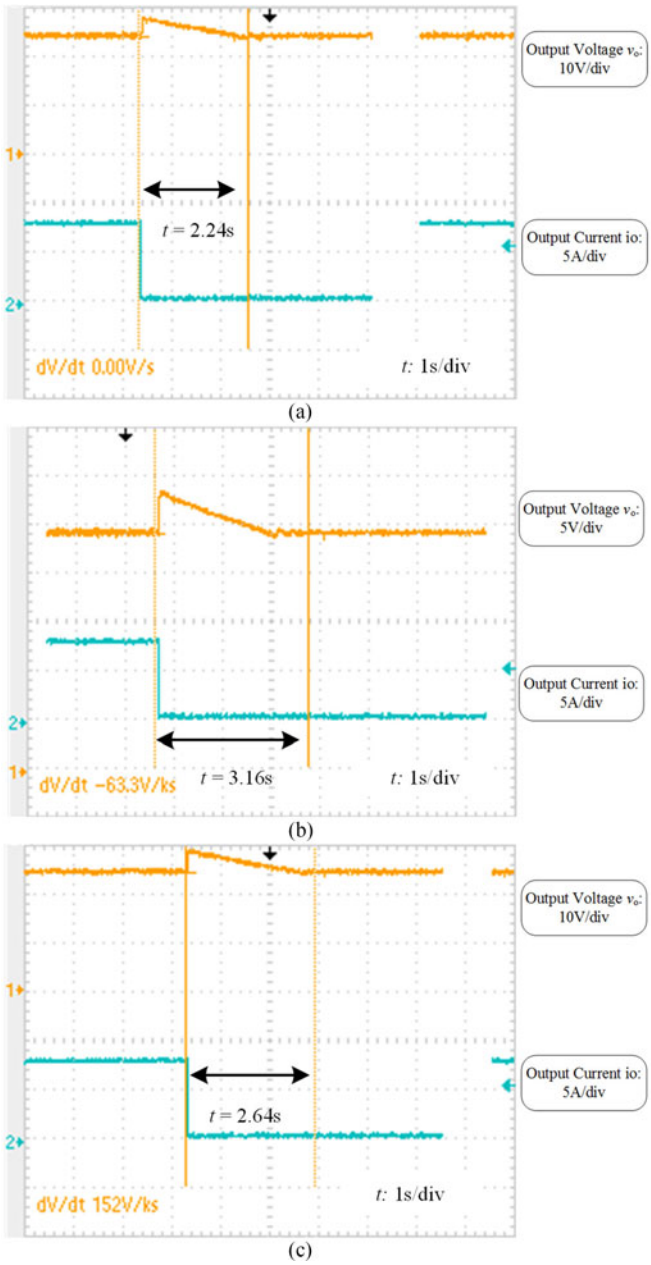

Fig. 19. Experimental results of *LLC* resonant converter against load step from full load to no load. (a) Case 1 with proposed strategy. (b) Case 2 with PI controller. (c) Case 3 with PI controller in switching frequency.

Fig 17 shows the experimental results against step load from half load to full load in the three cases. At half load condition, the switching frequency is near the resonant frequency to regulate the output voltage. The influence of junction and winding capacitor is eliminated. The dynamic response is faster than the condition that load step up from no load to full load. At case 1, the settling time is only 29 μs and the voltage drop is very small, near zero, as shown in Fig. 18(a). At case 2, the setting time is 44 μs. The output voltage nearly does not change. At case 3, the setting time is 22.5 ms. The voltage drop is 2.4 V and the voltage overshoot is 1.2 V. Since the output voltage may not reach at steady state at every switching period, the oscillations worsen the dynamic characteristics of an *LLC* resonant converter. The high control frequency near switching frequency can make the converter unstable.

TABLE II
DYNAMIC RESPONSE COMPARE WITH THREE CASES UNDER DIFFERENT CONDITIONS

Setting time	Case 1	Case 2	Case 3
Load step from no to full	20.4 ms	38.8 ms	41.2 ms
Load step from half to full	29 μs	44 μs	22.4 μs
Load step from full to half	28 μs	40 μs	19.2 μs
Load step from full to no	2.24 s	3.16 s	2.64 s

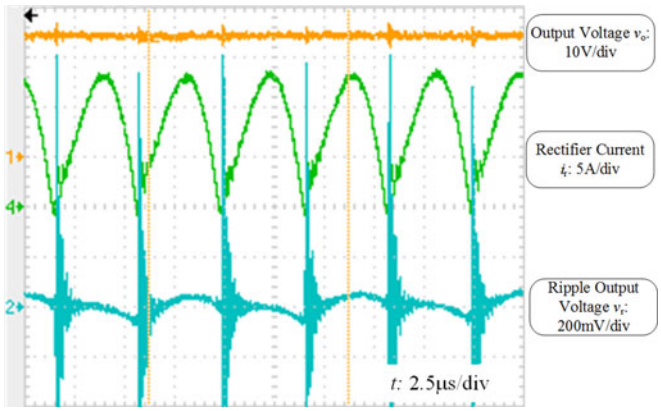

Fig. 20. Waveforms of ripple current and voltage.

Figs. 16 and 17 shows the experimental results of the *LLC* resonant converter against load step up. The results of converter against load step down are shown in Figs. 18 and 19. The dynamic response of the *LLC* resonant converter from full load to half is shown in Fig. 18. At case 1, the setting time is 28 μs, similar with load step up. At case 2, the setting time is 40 μs, as shown in Fig. 18(b). At case 3, the setting time is 19.2 ms due to the oscillation.

When the load step down from full to no load, output voltage will have a large overshoot. The converter operates at burst mode at beginning. Due to the higher voltage, all the switches stop working. The output voltage reduces to the reference value using the dead load. The setting time is very long, as shown in Fig. 19. At case 1, the setting time is 2.24 s and voltage overshoot is 4 V. At case 2, the setting time is 3.16 s and the overshoot is 4 V. The proposed strategy has a better dynamic response. At case 3, the setting time is 2.64 s and the overshoot is 4.4 V. The oscillation is eliminated since the converter works at the burst mode. The dynamic performance is improved due to the high control frequency.

Table II gives the setting time of the three cases under different conditions. The *LLC* resonant converter works at the burst mode with maximum switching frequency under on load condition. And the converter works near the resonant frequency at half load. Therefore, the setting time against load step up from no to full load is longer than the setting time from half to full load. At case 3, the higher control frequency, which is equal with the switching frequency, causes some oscillations during the loads' variation period. The dynamic response of case 3 is

worse than the case 2. Since the nonlinear characteristics are eliminated at case 1, the proposed control strategy has a best dynamic performance.

Fig. 20 shows the waveforms of ripple current and ripple voltage of the output capacitor. The yellow line is the output voltage and it has been regulated to 24 V. The blue line is the ripple voltage and due to large output capacitor value, the peak-peak value of ripple voltage is only 150 mV. Green line is the rectifier diode current and its peak-peak value is about 14 A. Thus, large output capacitors are needed to absorb the large ripple currents.

VI. Conclusion

This paper proposes a load feedback linearized control strategy of an *LLC* resonant converter to improve the performance. The nonlinear characteristics of the *LLC* resonant converter caused by the variable frequency control are eliminated. The dynamic response is improved. The settling time of the load step up from no to full load is reduced from 38.8 to 20.4 ms compared with the conventional PI controller. The main contributions of this paper are as follows.

1) Propose a load feedback linearization control strategy, which can effectively improve the dynamic performance of the *LLC* resonant converter. Using the loads feedback, the nonlinear characteristics are eliminated. The output characteristics can be regulated as expected.
2) Build a simple two-order model of an *LLC* resonant converter. Although ignoring the dynamic influence of the resonant network, the complex seven-order model of converter based on FHA is simplified as a two-order model. The *LLC* resonant converter can be equal as a controlled voltage source with a *LC* filter. This model is helpful to guide the design of the resonant converter's controller.

Experimental results verify the effectiveness of the proposed control strategy. And the proposed controller and modeling method can also be used for other resonant converters.

Appendix

v_m is the magnetic voltage of the *LLC* resonant converter. When the resonant current is larger than the magnetic current, the magnetic voltage is equal to the output voltage, provided that the turns ratio is 1; otherwise, the negative value of output voltage instead is

$$v_m = nv_o \cdot \operatorname{sign}(i_r - i_m)$$
$$\operatorname{sign}(i_r - i_m) = \begin{cases} 1 & i_r > i_m \\ -1 & i_r < i_m \end{cases}. \quad (35)$$

Since the resonant and magnetic current are both sinusoidal signals, the magnetic voltage is a square wave signal, which is half positive and half negative values and the waveform is similar with that of input voltage v_{ab} but with a difference in amplitude and phase. Then, the fundament component of magnetic voltage can be written as follows:

$$v_m = (4nv_o/\pi)\sin(\omega_s t + \varphi). \quad (36)$$

The phase difference is decided by the difference between resonant and magnetic current

$$i_r - i_m = i_p \sin(\omega_s t + \varphi)$$
$$= (i_{rs} - i_{ms})\sin\omega_s t + (i_{rc} - i_{mc})\cos\omega_s t. \quad (37)$$

Then, we have

$$\cos\varphi = (i_{rc} - i_{mc})/i_p;\ \sin\varphi = (i_{rs} - i_{ms})/i_p. \quad (38)$$

Therefore, the magnetic voltage can be derived as follows:

$$v_m = [4nv_o(i_{rs} - i_{ms})/(\pi i_p)]\sin\omega_s t + [4nv_o(i_{rc} - i_{mc})/(\pi i_p)]\cos\omega_s t. \quad (39)$$

References

[1] G. Ivensky, S. Bronshtein, and A. Abramovitz, "Approximate analysis of resonant LLC DC-DC converter," *IEEE Trans. Power Electron.*, vol. 26, no. 11, pp. 3274–3284, Nov. 2011.

[2] X. Mathu, C. O. Na, W. Ningning, S. Kulkarni, and S. Roy, "Review of integrated magnetics for power supply on chip (PwrSoC)," *IEEE Trans. Power Electron.*, vol. 27, no. 11, pp. 4799–4816, Nov. 2012.

[3] K. Bong-Chul, P. Ki-Bum, K. Chong-Eun, L. Byoung-Hee, and M. Gun-Woo, "LLC resonant converter with adaptive link-voltage variation for a high-power-density adapter," *IEEE Trans. Power Electron.*, vol. 25, no. 9, pp. 2248–2252, Sep. 2010.

[4] L. Huber, G. Liu, and M. M. Jovanovic, "Design-oriented analysis and performance evaluation of buck PFC front end," *IEEE Trans. Power Electron.*, vol. 25, no. 1, pp. 85–94, Jan. 2010.

[5] J. Cao and A. Emadi, "A new battery/ultra capacitor hybrid energy storage system for electric, hybrid, and plug-in hybrid electric vehicles," *IEEE Trans. Power Electron.*, vol. 27, no. 1, pp. 122–132, Jan. 2012.

[6] L. Wuhua and H. Xiangning, "Review of nonisolated high-step-up DC/DC converters in photovoltaic grid-connected applications," *IEEE Trans. Ind. Electron.*, vol. 58, no. 4, pp. 1239–1250, Apr. 2011.

[7] Q. Zhijun, O. Abdel-Rahman, H. Al-Atrash, and I. Batarseh, "Modeling and control of three-port DC/DC converter interface for satellite applications," *IEEE Trans. Power Electron.*, vol. 25, no. 3, pp. 637–649, Mar. 2010.

[8] A. Kwasinski and C. N. Onwuchekwa, "Dynamic behavior and stabilization of DC microgrids with instantaneous constant-power loads," *IEEE Trans. Power Electron.*, vol. 26, no. 3, pp. 822–834, Mar. 2011.

[9] M. Saeedifard and R. Iravani, "Dynamic performance of a modular multilevel back-to-back HVDC system," *IEEE Trans. Power Del.*, vol. 25, no. 4, pp. 2903–2912, Apr. 2010.

[10] L. Xiaodong and A. K. S. Bhat, "Analysis and design of high-frequency isolated dual-bridge series resonant DC/DC converter," *IEEE Trans. Power Electron.*, vol. 25, no. 4, pp. 850–862, Apr. 2010.

[11] Q. Ying, C. Xiyou, Z. Chongquan, and Q. Chen, "Uniform models of PWM DC-DC converters for discontinuous conduction mode considering parasitics," *IEEE Trans. Ind. Electron.*, vol. 61, no. 11, pp. 6071–6080, Nov. 2014.

[12] B. Yang, F. C. Lee, A. J. Zhang, and H. Guisong, "LLC resonant converter for front end DC/DC conversion," in *Proc. IEEE Appl. Power Electron. Conf. Expo.*, Mar. 2002, vol. 2, pp. 1108–1112.

[13] L. Bing, L. Wenduo, L. Yan, F. C. Lee, and J. D. Van Wyk, "Optimal design methodology for LLC resonant converter," in *Proc. IEEE Appl. Power Electron. Conf. Expo.*, Mar. 2006, pp. 533–538.

[14] M. P. Foster, C. R. Gould, A. J. Gilbert, D. A. Stone, and C. M. Bingham, "Analysis of CLL voltage-output resonant converters using describing functions," *IEEE Trans. Power Electron.*, vol. 23, no. 4, pp. 1772–1781, Apr. 2008.

[15] F. Zhijian, C. Tao, D. Shanxu, and C. Changsong, "Optimal design methodology for LLC resonant converter in battery charging applications based on time-weighted average efficiency," *IEEE Trans. Power Electron.*, vol. 30, no. 10, pp. 5469–5483, Oct. 2015.

[16] G. C. Verghese, M. E. Elbuluk, and J. G. Kassakian, "A general approach to sampled-data modeling for power electronic circuits," *IEEE Trans. Power Electron.*, vol. PE-1, no. 2, pp. 76–89, Feb. 1986.

[17] B. Yang, F. C. Lee, and M. Jovanovic, "Small-signal analysis for LLC resonant converter," Center Power Electron. Syst. Semin., 2003, pp. 144–149.

[18] C. Chien-Hsuan, C. En-Chih, C. Chun-An, C. Hung-Liang, and L. Sheng-Chang, "Small signal modeling of LLC resonant converters based on extended describing function," in *Proc. Int. Symp. Comput., Consum. Control*, Jun. 2012, pp. 365–368.
[19] J. Stahl, H. Steuer, and T. Duerbaum, "Discrete modeling of resonant converters steady state and small signal description," in *Proc. IEEE Energy Convers. Congr. Expo.*, Sep. 2012, pp. 1578–1584.
[20] B. Cheng, F. Musavi, and W. G. Dunford, "Novel small signal modeling and control of an LLC resonant converter," in *Proc. IEEE Appl. Power Electron. Conf. Expo.*, Mar. 2014, pp. 2828–2834.
[21] J. Jinhaeng, J. Minjae, C. Seokjae, C. Youngho, and C. Byungcho, "Current mode control for LLC series resonant dc-to-dc converters," in *Proc. IEEE Appl. Power Electron. Conf. Expo.*, Mar. 2011, pp. 21–27.
[22] J. Jinhaeng, P. S. Kumar, K. Dongyun, and C. Byungcho, "Average current-mode control for LLC series resonant dc-to-dc converters," in *Proc. Power Electron. Motion Control Conf.*, Jun. 2012, vol. 2, pp. 923–930.
[23] Z. Sheng, L. Haoze, L. Wuhua, H. Xiangning, and X. Changliang, "Theoretical evaluation of stability improvement brought by resonant current loop for paralleled LLC converters," *IEEE Trans. Ind. Electron.*, vol. 62, no. 7, pp. 4170–4180, Jul. 2015.
[24] X. Fan, Z. Bo, and Q. Dongyuan, "Stabilizing the nonlinear dynamic behavior of LLC resonance full-bridge DC-DC converter under voltage mode control," in *Proc. Electron. Appl. Conf. Expo.*, Nov. 2014, pp. 1093–1097.
[25] O. Dranga, B. Buti, and I. Nagy, "Stability analysis of a feedback-controlled resonant DC-DC converter," *IEEE Trans. Ind. Electron.*, vol. 50, no. 1, pp. 141–152, Jan. 2003.
[26] K. Mandal, S. Banerjee, and C. Chakraborty, "Determination of stable region of controller parameters for series-parallel resonant converter with capacitive output filter," in *Proc. IEEE Int. Symp. Ind. Electron.*, Jun. 2011, pp. 229–232.
[27] J. Jinhaeng, J. Minjae, C. Byungcho, and K. Heung-Geun, "Dynamic analysis and control design of optocoupler-isolated LLC series resonant converters with wide input and load variations," in *Proc. IEEE Energy Convers. Congr. Expo.*, Sep. 2009, pp. 758–765.
[28] F. Kurokawa and K. Murata, "A new quick response digital modified P-I-D control LLC resonant converter for DC power supply system," in *Proc. IEEE Power Electron. Drive Syst.*, Dec. 2011, pp. 35–39.
[29] L. Chun-Liang, C. Yi-Hsun, L. Yi-Feng, W. Shun-Chung, and L. Yi-hua, "Design and implementation of a digitally-controlled LLC resonant converter for battery charging applications," in *Proc. IEEE Power Electron. Drive Syst.*, Apr. 2013, pp. 804–808.
[30] M. I. Shahzad, S. Iqbal, and S. Taib, "LLC series resonant converter with PID controller for battery charging application," in *Proc. IEEE Energy Convers.*, Oct. 2014, pp. 84–89.
[31] C. Buccella, C. Cecati, H. Latafat, P. Pepe, and K. Razi, "Observer-based control of LLC DC/DC resonant converter using extended describing functions," *IEEE Trans. Power Electron.*, vol. 30, no. 10, pp. 5881–5891, Oct. 2015.
[32] M. Hao, L. Qinwei, and G. Jin, "A sliding-mode control scheme for LLC resonant DC/DC converter with fast transient response," in *Proc. IEEE Energy Convers.*, Oct. 2012, pp. 162–167.
[33] H. Zhiyuan, W. Laili, L. Yan-Fei, and P. C. Sen, "Bang-Bang charge control for LLC resonant converters," in *Proc. IEEE Energy Convers. Congr. Expo.*, Sep. 2013, pp. 140–146.
[34] T. Nishimura *et al.*, "Robust digital control for an LLC current-resonant DC-DC converter," in *Proc. Elect. Eng./Electron., Comput., Telecommun. Inf. Technol.*, May 2012, pp.1–4.
[35] C. L. Chia and E. K. K. Sng, "A novel robust control method for the series–parallel resonant converter," *IEEE Trans. Power Electron.*, vol. 24, no. 8, pp. 1896–1904, Aug. 2009.
[36] F. Weiyi, F. C. Lee, and P. Mattavelli, "Optimal trajectory control of burst mode for LLC resonant converter," *IEEE Trans. Power Electron.*, vol. 28, no. 1, pp. 457–466, Jan. 2013.
[37] F. Weiyi, F. C. Lee, and P. Mattavelli, "Simplified optimal trajectory control (SOTC) for LLC resonant converters," *IEEE Trans. Power Electron.*, vol. 28, no. 5, pp. 2415–2426, May 2013.
[38] F. Weiyi and F. C. Lee, "Optimal trajectory control of LLC resonant converters for soft start-up," *IEEE Trans. Power Electron.*, vol. 29, no. 3, pp. 1461–1468, Mar. 2014.
[39] F. Weiyi, F. C. Lee, and P. Mattavelli, "Optimal trajectory control of LLC resonant converters for LED PWM dimming," *IEEE Trans. Power Electron.*, vol. 29, no. 2, pp. 979–987, Feb. 2014.
[40] B. Yang, "Topology investigation of front end DC/DC converter for distributed power system," Ph.D. dissertation, , Virginia Tech, Blacksburg, VA, USA, Sep. 2003.

Zhijian Fang received the B.S. and Ph.D. degrees in electrical engineering and automation from Huazhong University of Science and Technology, Wuhan, China, in 2010 and 2015, respectively.

Since 2015, he has been a Postdoctoral Research Fellow in the School of Electrical Engineering, Wuhan University, Wuhan, China. From February 2016 to January 2017, he was a Postdoctoral Research Fellow with Department of Electrical and Computer Engineering, Ryerson University, Toronto, ON, Canada. His research interests include high performance dc/dc converter, battery charger, and renewable energy applications.

Junhua Wang was born in Shandong, China, in 1981. He received the Ph.D. degree in Electrical Engineering from Hong Kong Polytechnic University, Hong Kong, China, in 2012.

He joined the Carnegie Mellon University as a Postdoctoral Researcher in 2012 and then worked as a Research Fellow in the GATE Center for Electric Drive Transportation, Dearborn, MI, USA. He is currently a Professor in the School of Electrical Engineering, Wuhan University, Wuhan, China. His research interests include wireless transmission technology based on magnetic resonance, applied electromagnetics, system equipment for power transmission and distribution.

Shanxu Duan received the B.S., M.S., and Ph.D. degrees in electrical engineering from Huazhong University of Science and Technology, Wuhan, China, in 1991, 1994, and 1999, respectively.

Since 1991, he has been a Faculty Member in the School of Electrical and Electronics Engineering, Huazhong University of Science and Technology, Wuhan, China, where he is currently a Professor. His research interests include stabilization, nonlinear control with application to power electronic circuits and systems, fully digitalized control techniques for power electronics apparatus and systems, and optimal control theory and corresponding application techniques for high frequency pulse width modulation power converters.

Dr. Duan is a Senior Member of the Chinese Society of Electrical Engineering and a council member of the Chinese Power Electronics Society. He was selected as one of the New Century Excellent Talents by the Ministry of Education of China in 2007. He received the honor of "Delta Scholar" in May 2009.

Kaipei Liu was born in Hubei, China, in 1962. He received the Ph.D. degree in computer application technology from Wuhan University, Wuhan, China, in 2001.

He is currently a Professor in the School of Electrical Engineering, Wuhan University, where he has been researching power electronics technology.

Tao Cai was born in Hubei Province, China, in 1974. He received the Ph.D. degree in control science and engineering from Huazhong University of Science and Technology, Wuhan, China, in 2004.

His research interests include advanced signal processing and energy management of renewable power generation. He has authored about 20 technical papers in journal and conferences.